Epidemics 33 (2020) 100406

Contents lists available at ScienceDirect

Epidemics

journal homepage: www.elsevier.com/locate/epidemics

Quantifying mechanistic traits of influenza viral dynamics using in vitro data

Ada W.C. Yan [a], Jie Zhou [b], Catherine A.A. Beauchemin [c,d], Colin A. Russell [e], Wendy S. Barclay [b], Steven Riley [a,*]

[a] MRC Centre for Global Infectious Disease Analysis, Department of Infectious Disease Epidemiology, School of Public Health, Imperial College London, London W2 1PG, United Kingdom
[b] Section of Virology, Department of Medicine, Imperial College London, London W2 1PG, United Kingdom
[c] Department of Physics, Ryerson University, 350 Victoria Street, Toronto, Ontario, M5B 2K3, Canada
[d] Interdisciplinary Theoretical and Mathematical Sciences (iTHEMS), RIKEN, 2-1 Hirosawa, Wako, Saitama, 351-0198, Japan
[e] Laboratory of Applied Evolutionary Biology, Department of Medical Microbiology, Academic Medical Center, University of Amsterdam, Meibergdreef 9, Amsterdam, 1105 AZ, The Netherlands

ARTICLE INFO

Keywords:
Mathematical model
Viral dynamics
Influenza

ABSTRACT

When analysing *in vitro* data, growth kinetics of influenza virus strains are often compared by computing their growth rates, which are sometimes used as proxies for fitness. However, analogous to mathematical models for epidemics, the growth rate can be defined as a function of mechanistic traits: the basic reproduction number (the average number of cells each infected cell infects) and the mean generation time (the average length of a replication cycle). Fitting a model to previously published and newly generated data from experiments in human lung cells, we compared estimates of growth rate, reproduction number and generation time for six influenza A strains. Of four strains in previously published data, A/Canada/RV733/2003 (seasonal H1N1) had the lowest basic reproduction number, followed by A/Mexico/INDRE4487/2009 (pandemic H1N1), then A/Indonesia/05/2005 (spill-over H5N1) and A/Anhui/1/2013 (spill-over H7N9). This ordering of strains was preserved for both generation time and growth rate, suggesting a positive biological correlation between these quantities which have not been previously observed. We further investigated these potential correlations using data from reassortant viruses with different internal proteins (from A/England/195/2009 (pandemic H1N1) and A/Turkey/05/2005 (H5N1)), and the same surface proteins (from A/Puerto Rico/8/34 (lab-adapted H1N1)). Similar correlations between traits were observed for these viruses, confirming our initial findings and suggesting that these patterns were related to the degree of human adaptation of internal genes. Also, the model predicted that strains with a smaller basic reproduction number, shorter generation time and slower growth rate underwent more replication cycles by the time of peak viral load, potentially accumulating mutations more quickly. These results illustrate the utility of mathematical models in inferring traits driving observed differences in *in vitro* growth of influenza strains.

1. Introduction

The initial growth rate is often directly interpreted in studies of virus evolution as a measure of *in vitro* or within-host fitness (Sanjuán, 2010; Lyons and Lauring, 2018). In epidemiological studies, the initial growth rate can be expressed as a function of two parameters: the basic reproduction number and the mean generation time (Nishiura et al., 2010; Wallinga and Lipsitch, 2007). Each of these concepts can also be applied to the *in vitro* or within-host context, but only the growth rate is commonly used in experimental virology to characterise *in vitro*/within-host growth kinetics.

The basic reproduction number in an epidemiological context is the mean number of secondary infections due to an initial infected individual in an otherwise susceptible population. The cellular-level equivalent is the mean number of secondary infected cells due to an initial infected cell in an otherwise susceptible cell population. Studies have estimated the basic cellular reproduction number for different pathogens, such as HIV/SHIV (Nowak and Bangham, 1996; Iwami et al., 2012, 2015; Iwanami et al., 2017), influenza A virus (Möhler et al., 2005; Baccam et al., 2006) and rotavirus (González-Parra et al., 2018). A limited number of these studies have directly compared the basic reproduction number between different influenza or SHIV strains, as a measure of relative fitness (Mitchell et al., 2011; Iwanami et al., 2017; Farrukee et al., 2018).

* Corresponding author.
E-mail address: s.riley@imperial.ac.uk (S. Riley).

https://doi.org/10.1016/j.epidem.2020.100406
Received 19 October 2019; Received in revised form 10 July 2020; Accepted 4 September 2020
Available online 3 October 2020

In an epidemiological context, the generation time is the time between infection of an individual and infection of a secondary case. The cellular-level equivalent is the time between infection of a cell and infection of a secondary cell. Since a single cell will infect many secondary cells, this time varies between pairs of primary and secondary infected cells. A useful summary statistic for the distribution of these times is the mean generation time averaged over all secondary cells, in an otherwise susceptible cell population. The mean generation time is an important parameter in models of pathogen evolution (Russell et al., 2012; Fonville, 2015; Illingworth, 2015; Nené et al., 2018; Geoghegan et al., 2016; Reperant et al., 2015). In the context of HIV, a mean generation time on the order of days has been linked to the rapid evolution of drug resistance, necessitating combination antiretroviral therapy (Perelson et al., 1996). Although mechanistic models have been used to quantify the mean generation time for HIV (Perelson et al., 1996; Iwami et al., 2015; Althaus et al., 2009; Dixit et al., 2004), the effects of between-strain differences on the dynamics of infection and evolution are not well studied.

This study aims to highlight the utility of the basic reproduction number and mean generation time in addition to the initial growth rate in considering the dynamics of an acute infection. We find that strains with a small basic reproduction number also tend to have a short mean generation time and a slow initial growth rate, a biological correlation which has not previously been observed. We then use simulations to show the impact of these parameters on the number of replication rounds leading up to peak shedding; slower initial growth rates lead to a greater proportion of virions that were the product of several replication rounds. We anticipate that strain differences in the number of replication cycles changes the accumulation rate of multiple mutations within a single infection, with consequences for the pace of virus evolution.

2. Methods

2.1. Strains with wild-type HA and NA

We re-analysed data published by Simon et al. (2016). In brief, A/Canada/RV733/2003 (sH1N1-WT), A/Mexico/INDRE4487/2009 (pH1N1-WT), A/Indonesia/05/2005 (H5N1-WT) and A/Anhui/1/2013 (H7N9-WT) stocks were grown in MDCK cells. Single-cycle and multi-cycle experiments were carried out in triplicate in A549 human lung carcinoma cells in T25 flasks. Cells were infected at multiplicity of infection (MOI) = 3 and MOI = 0.01 for the single-cycle and multi-cycle experiments respectively, for an incubation period of 1 h at 37 °C. For the single-cycle experiment, the cells were washed with an acidic saline wash after the incubation period. At set time points, 0.5 mL of the 10 mL supernatant volume was harvested and replaced with 0.5 mL of fresh media. A mock-yield experiment was also performed in triplicate, where 10^7 plaque forming units (pfu) of each strain was left to decay in cell-free media incubated at 37 °C. Infectious virus was quantified using a $TCID_{50}$ assay, and for the single-cycle and multi-cycle experiments, total virus was quantified using qRT-PCR.

2.2. Strains with A/Puerto Rico/8/34 (PR8) HA and NA

Human embryonic kidney (293T) (ATCC), human lung adenocarcinoma epithelial cells (A549) (ATCC) and Madin–Darby canine kidney (MDCK) cells (ATCC) cells were maintained in Dulbecco's modified Eagle's medium (DMEM; Gibco, Invitrogen) supplemented with 10% fetal calf serum, 1% non-essential amino acids and 1% penicillin–streptomycin (5000 IU/mL; 5000 μL) at 37 °C and 5% CO_2.

We generated two reverse genetics viruses (pH1N1-PR8 and H5N1-PR8). In these viruses, the HA and NA genes were from the laboratory adapted strain A/Puerto Rico/8/34 (PR8, H1N1), and the six remaining gene segments were from either A/England/195/2009 (pH1N1) or A/Turkey/05/2005 (H5N1). Eight poll plasmids encoding the indicated virus segments and four helper expression plasmids encoding polymerase components and NP expressed by the pCAGGS vector were transfected into 293T cells. After 24 h, the transfected 293T cells were resuspended and co-cultured with MDCK cells. Virus stocks were thus grown on MDCK cells using serum free DMEM supplemented with 1 μg/mL of TPCK trypsin (Worthington). Viruses were stored in −80 °C and titrated on MDCK cells by plaque assay to determine the dilution required to achieve a given multiplicity of infection.

All infection experiments were performed in triplicate (three wells on the same plate). For the single-cycle and multi-cycle experiments, A549 cells were plated in a six-well plate (2.5×10^6 cells per well). One day after plating, medium was removed from cells and cells were washed twice with PBS (3 mL/well), then covered with 500 μL serum-free DMEM medium. Cells were infected at MOI = 5 and MOI = 0.01 for the single-cycle and multi-cycle experiments respectively; the virus was thawed in a 37 °C water bath, then diluted with serum-free DMEM to a volume of 500 μL. After an incubation period of one hour, the inoculum was removed, cells were washed four times with 3 mL serum-free DMEM, and 3 mL serum-free DMEM with 1 μg/mL TPCK-treated trypsin was added to each well (without cells). At each measurement time (shown in Fig. 2), the plates were shaken and 300 μL supernatant was collected, and replaced by 300 μL serum-free DMEM with 1 μg/mL TPCK-treated trypsin. The supernatant was frozen at −80 °C for later quantification. For the mock-yield experiments, 3 mL of virus at concentration 10^7 pfu/mL was added to each well. At each measurement time, 300 μL supernatant was collected without replacement and frozen at −80 °C for later quantification.

Plaque assays were carried out in confluent monolayers of MDCK cells in 12-well plates. 100 μL of each tenfold virus dilution was applied to each cell and incubated for 1 h at 37 °C. The inoculum was then removed, and the cells were overlaid with 0.6% agarose in MEM including 1 μg/mL TPCK-treated trypsin and 0.3% bovine serum albumin fraction V (Gibco). The cells were then incubated at 37 °C. After 3 days, the agarose was removed and the cells stained with 1 mL 0.5% crystal violet.

2.3. Mathematical model

Our mechanistic model (Fig. 1) is formulated as a set of ordinary differential equations:

$$\frac{dT}{dt} = -\beta T V_{inf}, \tag{1a}$$

$$\frac{dL_1}{dt} = \beta T V_{inf} - \frac{n_L}{\tau_L} L_1, \tag{1b}$$

$$\frac{dL_i}{dt} = \frac{n_L}{\tau_L}(L_{i-1} - L_i), \qquad i = 2, \ldots, n_L, \tag{1c}$$

$$\frac{dI_1}{dt} = \frac{n_L}{\tau_L} L_{n_L} - \frac{n_I}{\tau_I} I_1, \tag{1d}$$

$$\frac{dI_j}{dt} = \frac{n_I}{\tau_I}(I_{j-1} - I_j), \qquad j = 2, \ldots, n_I, \tag{1e}$$

$$\frac{dV_{inf}}{dt} = p_{inf} \sum_{j=1}^{n_I} I_j - c_{inf} V_{inf} - \beta T V_{inf} n/S, \tag{1f}$$

$$\frac{dV_{RNA}}{dt} = p_{RNA} \sum_{j=1}^{n_I} I_j - c_{RNA} V_{RNA} - \beta T V_{RNA}/S, \tag{1g}$$

The model equations are based on the study by Simon et al. (2016) with modifications to account for loss of virus due to entry into target cells (Handel et al., 2007). The model structure was first used by Perelson et al. (1996) to model HIV infection, and first applied to influenza infection by Baccam et al. (2006). It includes the following processes:

- infection of a target cell (T) by infectious virus (V_{inf}) at rate β;

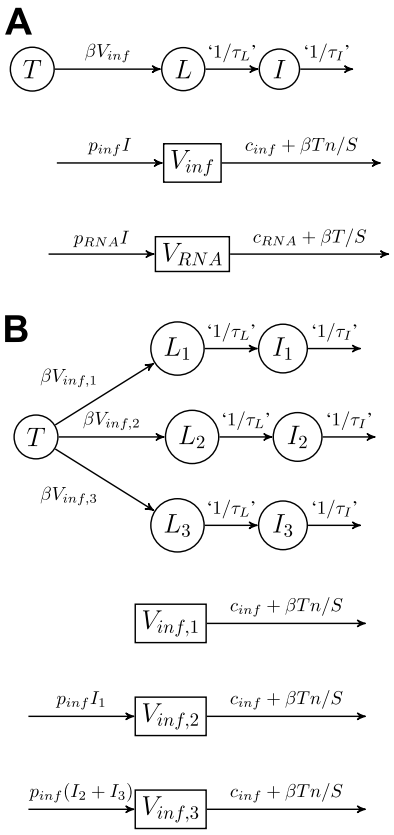

Fig. 1. (A) Viral dynamics model; (B) Model tracking generation number. Circles indicate cell compartments, while squares denote virion compartments. Quotation marks indicate that the waiting time between compartments is gamma-distributed rather than exponentially distributed, and that the mean waiting time is the inverse of the 'rate' given. (B) illustrates $N = 3$ generations.

- an infected cell (L) entering a state of virion production (I, where τ_L is the mean time spent in the latent period between infection and the state of virion production);
- production of infectious and non-infectious virions (to be explained in further detail);
- death of infected cells (τ_I is the mean time from entering the state of virion production to death);
- loss of virus due to entry into target cells (n and S are associated conversion constants as detailed in the Supplementary Material);
- loss of infectivity of free infectious virions at rate c_{inf}; and
- degradation of free total virions at rate c_{RNA}.

The infected cells pass through n_L latent stages and n_I infectious stages, where the duration of each stage is exponentially distributed. As a result, the latent and infectious periods are Erlang distributed, as per previous studies (Pinilla et al., 2012; Beggs and Dobrovolny, 2015; Petrie et al., 2013; Liao et al., 2016; Paradis et al., 2015; Beauchemin et al., 2017). Holder and Beauchemin (2011) showed that for influenza, compared to exponentially distributed latent and infectious periods, normally distributed or lognormally distributed latent and infectious periods lead to better fits to single-cycle data. When the shape parameter is much greater than 1, the Erlang distribution is similar in shape to the normal and lognormal distributions. Infectious and total (infectious plus non-infectious) viral load are represented by V_{inf} and V_{RNA} respectively. They are produced from infected cells at rates p_{inf} and p_{RNA} respectively. We do not model time-dependent effects of the immune response. Model compartments and parameters are summarised in Table 1.

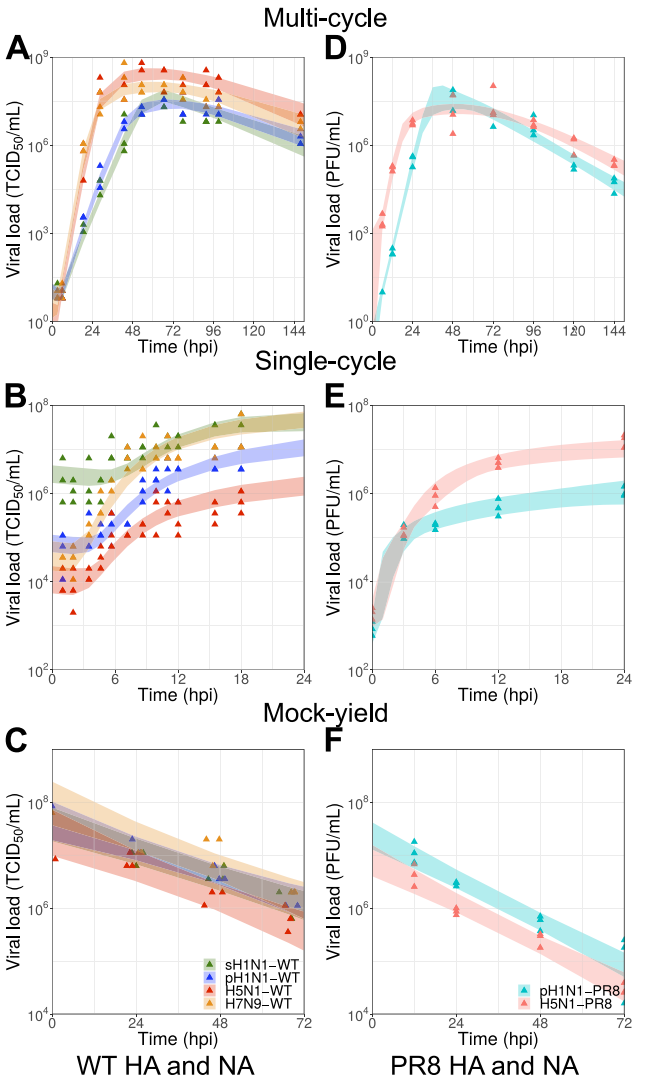

Fig. 2. Model fits to experimental data. The infectious viral load for the WT strains (A–C) and the strains with PR8 HA and NA (D–F). Fitted 95% credible intervals are shown as shaded areas on top the data (triangles). The infectious viral load is shown for (from top) the multi-cycle experiments, the single-cycle experiments and the mock-yield experiments. Note that data points in (C) are plotted as jittered in the horizontal direction to reduce overlap.

We do not observe V_{RNA} for the strains with PR8 HA and NA, so we omit the last equation for these strains.

Single-cycle, multi-cycle and mock-yield experiments can be simulated using this model by changing the initial conditions. Single-cycle and multi-cycle experiments start with a fixed number of target cells T_0, and infectious and total virus at high (for single-cycle) or low (for multi-cycle) values. Mock-yield experiments start with no target cells and a large amount of infectious virus.

The basic reproduction number for this model is

$$R_0 = \frac{\beta T_0 p_{inf} \tau_I}{c_{inf} + \beta T_0 n/S}; \tag{2}$$

the mean generation time, which we consider in the context of a fully susceptible population, is

$$T_G = \tau_L + \frac{n_I + 1}{2n_I}\tau_I + \frac{1}{c + \beta T_0 n/S}; \tag{3}$$

and the initial growth rate r is computed by linearising around the disease-free equilibrium $[T, L_i, I_i, V_{inf}] = [T_0, 0, 0, 0]$ (Nowak et al., 1997; Lee et al., 2009).

Table 1
Compartment and parameter definitions.

Compartment/Parameter	Definition	Units
T	Target cell	cell
L	Infected cell not yet producing virus	cell
I	Infected cell producing virus	cell
V_{inf}	Infectious virus	u_V/mL (see note)
V_{RNA}	Total virus	RNA copy number/mL
β	Rate at which virus infects cells	u_V^{-1}mL h^{-1}
p_{inf}	Infectious virus production rate	u_V/mL (cell^{-1}) h^{-1}
p_{RNA}	Total virus production rate	RNA copy number/mL (cell^{-1}) h^{-1}
c_{inf}	Rate of loss of infectivity of free virus	h^{-1}
c_{RNA}	Viral RNA degradation rate	h^{-1}
τ_L	Mean latent period	h
τ_I	Mean infectious period	h
n_L	Number of latent stages	–
n_I	Number of infectious stages	–
n	Amount of u_V entering each cell upon infection	u_V/cell
S	Supernatant volume	mL

Note: The infectious virus unit u_V is $TCID_{50}$ for the WT experiments and pfu for the PR8 experiments.

We model observation error as lognormal, with an observation threshold at low titres. Further details of the model are in the Supplementary Material.

2.4. Parameter estimation

Parameters were estimated for each strain separately using an adaptive Metropolis–Hastings algorithm. For a given strain, parameters were estimated using combined data from the multi-cycle, single-cycle and mock yield experiments. For a given strain, these experiments share all model parameters except for the production rate of infectious virus p_{inf}, and otherwise differ only in initial conditions. p_{inf} for the single-cycle experiments is modelled as lower (or equal to) that for the multi-cycle experiments, to account for decreased infectious viral production due to the presence of defective interfering particles at a high multiplicity of infection (Simon et al., 2016). We do so by introducing two parameters for virus production — $p_{inf,SC}$ and $p_{inf,MC}$ — and fitting both $p_{inf,MC}$ and $p_{inf,SC}/p_{inf,MC}$. $p_{inf,SC}/p_{inf,MC}$ is restricted to take values less than 1.

The viral RNA degradation rate, shape parameters of the latent period and viral production period distributions, initial number of target cells, supernatant volume and observation threshold were fixed. All other parameter values, including initial conditions, were estimated. A multi-dimensional uniform distribution was used as the prior, with some parameters log-transformed. Tables showing the fixed parameter values and the priors for the estimated parameters are included in the Supplementary Material.

2.5. Statistical analysis

For each pair of viruses in the study, for each estimated parameter, we computed the ratio of the virus-specific parameter values, and tested for deviations of the ratio from 1. For each parameter, p-values for each virus pair were computed by sampling with replacement from each marginal posterior distribution, and letting q be the proportion of sampled pairs whose ratio exceeds 1. The p-value was then $p = 2(min(q, 1-q))$. The strains with wild-type HA and NA were only compared to each other, and not to the strains with PR8 HA and NA.

2.6. Model with generation numbers

We extended our model to explicitly associate each virion and infected cell with a generation number. The inoculum was denoted virus generation 1, the cells infected by the inoculum denoted cell generation 1, the infectious virions produced by those cells denoted virus generation 2, and so forth. This model enables us to calculate the proportion of virions from each generation at a given time. The model with generations is illustrated in Fig. 1B for tracking $N = 3$ generations; the actual implementation tracks 20 generations. (Cells and virions above generation N are lumped into the generation N compartments). The bulk dynamics of the model remain the same, that is, the number of cells in L in Fig. 1A is equal to the sum of the numbers of cells in L_1, L_2 and L_3 in Fig. 1B, and similarly for I and V_{inf}. Model equations are as follows:

$$\frac{dT}{dt} = -\beta T \sum_{g=1}^{G} V_{inf,g}, \tag{4a}$$

$$\frac{dL_{1,g}}{dt} = \beta T V_{inf,g} - \frac{n_L}{\tau_L} L_{1,g}, \qquad g = 1, \dots, G, \tag{4b}$$

$$\frac{dL_{i,g}}{dt} = \frac{n_L}{\tau_L}(L_{i-1,g} - L_{i,g}), \qquad i = 2, \dots, n_L, g = 1, \dots, G, \tag{4c}$$

$$\frac{dI_{1,g}}{dt} = \frac{n_L}{\tau_L} L_{n_L,g} - \frac{n_I}{\tau_I} I_{1,g}, \qquad g = 1, \dots, G, \tag{4d}$$

$$\frac{dI_{j,g}}{dt} = \frac{n_I}{\tau_I}(I_{j-1,g} - I_{j,g}), \qquad j = 2, \dots, n_I, g = 1, \dots, G, \tag{4e}$$

$$\frac{dV_{inf,1}}{dt} = -c_{inf} V_{inf,1} - \beta T V_{inf,1} n/S, \tag{4f}$$

$$\frac{dV_{inf,g}}{dt} = p_{inf} \sum_{j=1}^{n_I} I_{j,g-1} - c_{inf} V_{inf,g} - \beta T V_{inf,g} n/S, \qquad g = 2, \dots, G-1, \tag{4g}$$

$$\frac{dV_{inf,G}}{dt} = p_{inf} \sum_{j=1}^{n_I} (I_{j,G-1} + I_{i,G}) - c_{inf} V_{inf,G} - \beta T V_{inf,G} n/S. \tag{4h}$$

Here, g denotes the generation number, and G is the maximum number of generations tracked, which is capped for computational purposes at $G = 20$. We solve the equations for the maximum likelihood parameters for a given strain, using multi-cycle initial conditions, to determine the peak viral load and infectious virion distribution at that time.

Data and code to reproduce all results can be found at https://github.com/ada-w-yan/cellularfluparams.

3. Results

We estimated model parameters for the four influenza A strains with wild-type HA and NA. The model accurately captured key features of the viral load (Fig. 2). With a low inoculum (MOI = 0.01), multiple generations of infection depleted the pool of susceptible cells over a period of 6 days resulting in an infectious viral load curve showing exponential growth, followed by a peak and exponential decay (Fig. 2A). With a larger inoculum (MOI = 3), most cells were infected immediately and the concentration of infectious virus plateaued earlier (Fig. 2B). The loss of infectivity of free virus was captured by the mock-yield assays where no cells were present (Fig. 2C). The model was also able to reproduce the observed total viral load patterns as quantified by qRT-PCR, although the viral load toward the end of the single-cycle experiments was slightly underestimated for the sH1N1-WT and pH1N1-WT strains (Fig. S1).

We hypothesise that our model cannot capture the continually increasing ratio between total and infectious viral load because the ratio between production rates of infectious and total virus is assumed to be constant, and we have assumed that only infectious virus affects infection dynamics. In reality, virus which is not measured by the $TCID_{50}$ assay could be semi-infectious or defective interfering particles — the latter of which are more abundant in single-cycle compared to multi-cycle infections, complicating the relationship between infectious and total viral load. Our model also assumes that only one virus can infect a cell; this assumption may not be true towards the end of single-cycle infections as the multiplicity of infection gets higher, and could affect the model's ability to explain the data. Investigating this hypothesis by explicitly modelling the dynamics of semi-infectious and/or defective interfering particles, and modelling multiply–infected cells is the subject of future work (see e.g. Liao et al. (2016), Koelle et al. (2019)). We also note some variation in the estimated viral load between strains at $t = 0$, despite the inoculum being the same between strains in the experimental protocol. This is possibly due to differences in inoculation efficiency which are not captured by our model, and we allow initial conditions to vary between strains to compensate.

Fig. 2D–F show data for experiments conducted with pH1N1-PR8 and H5N1-PR8, which were motivated by the analyses of the model fits to WT data in Figs. 3A–C. The model also fits these data well.

Supplementary Data S1 shows estimated model parameter values and the correlations between them.

From the estimated model parameters, we then calculated three traits — the basic reproduction number, the mean generation time and the initial growth rate for the four strains. We estimated the mean generation time to be between 25 and 65 h for the four WT strains, ranging from 32 h (median; 95% CI 27 h–40 h) for sH1N1-WT to 55 h (median; 95% CI 42 h–65 h) for H7N9-WT (Fig. 3A, left side of panel). There appeared to be an increasing trend in mean generation time from the strain most adapted to humans (sH1N1-WT) to the strain least adapted to humans (H7N9-WT). Strain differences were also observed in the basic reproduction numbers and initial growth rates (Figs. 3B–C). Supplementary Data S2 shows the median and 95% credible intervals plotted in Fig. 3. We note that combining data from three sets of experimental conditions (multi-cycle, single-cycle and mock-yield) enabled us to estimate these traits accurately. Fig. S2 shows that estimates using multi-cycle data only are less precise.

Fig. 3D further illustrates with a two-dimensional plot that strains with a high basic reproduction number also tended to have a long mean generation time. The same initial growth rate can be achieved via two different routes: a high basic reproduction number and a long mean generation time, or a low basic reproduction number and a short mean generation time (Nishiura et al., 2010; Wallinga and Lipsitch, 2007). High basic reproduction numbers and short mean generation times would lead to very high initial growth rates, while low basic reproduction numbers and long mean generation times would lead to very slow initial growth rates; these extreme values may not be biologically plausible. Because the basic reproduction number and the mean generation time are not completely independent, some types of data do not enable independent estimation of both traits, such that their marginal distributions are not well-constrained (Nishiura et al., 2010). This was not the case for our data. For each strain, there was indeed some correlation in the posterior distribution between the basic reproduction number and the mean generation time (Fig. S3; see also the diagonally stretched posterior distributions in Fig. 3D). Despite this correlation, the marginal distributions were still well-constrained, enabling differences to be seen between the estimated values for each strain (Figs. 3A–B, D).

We then investigated whether one of these three traits alone (the basic reproduction number, mean generation time and initial growth rate) could capture the observed differences between strains. We found that each trait summarised changes in a different set of infection processes, and thus offers a complementary perspective on viral dynamics. Fig. S4 shows the sensitivity of each trait to changes in the rates of underlying model parameters. For example, the leftmost bar shows the percentage change in the mean generation time for sH1N1-WT, if the infectivity of virions β were changed to that of H7N9-WT. We see that the basic reproduction number was mostly affected by changes in the mean infectious period τ_I and the infectivity β; the mean generation time was mostly affected by changes in τ_I; and the initial growth rate was mostly affected by changes in β. Note that unlike the epidemiological SIR model, the basic reproduction number, mean generation time and initial growth rate in a viral dynamics model with latent period are functions of up to five parameter combinations — βT_0, p_{inf}, τ_L, τ_I, and $c_{inf} + \beta T_0 n/S$. As a result, the values of any two traits do not uniquely determine the third.

We hypothesised that the differences between strains were driven by the internal proteins. To test this hypothesis, we conducted the same analysis on the pH1N1-PR8 and H5N1-PR8 data previously shown in Fig. 2D–F. The mean generation time for H5N1-PR8 was longer than that for pH1N1-PR8 (Fig. 3A, right side of panel). The median estimate of the basic reproduction number was also higher for H5N1-PR8 than pH1N1-PR8, although the difference was not statistically significant (Fig. 3B). Nevertheless, a positive correlation between basic reproduction number and mean generation time was observed (Fig. 3E), consistent with our previous results. The initial growth rate did not appear to be different between the strains (Fig. 3C), but the estimate for H5N1-PR8 was imprecise because few observations were made during the exponential growth phase of the multi-cycle experiment, as the viral load plateaued earlier than expected (Fig. 2F). Note that we did not compare the traits directly between pH1N1-WT and pH1N1-PR8, or between H5N1-WT and H5N1-PR8, because our interest is in the difference between the internal proteins of pH1N1 and H5N1, rather than the changes introduced to each strain by changing their surface proteins.

Simulations using the estimated parameters showed that by the peak time of infection, strains with a smaller basic reproduction number, shorter generation time and slower growth rate had a higher proportion of virions with a large generation number, which we define as one plus the number of replication cycles between the inoculum and the virion's production. The time of peak infectious viral load is of interest because in an *in vivo* infection, transmission is most likely around the time of peak viral load (Carrat et al., 2008). To perform these simulations, we extended our model to associate each infectious virion and infected cell with a generation number (see Methods). Fig. 4 shows the proportion of virions in each generation at the time of peak infectious viral load, according to the maximum likelihood parameter set for each strain, under multi-cycle experiment conditions. For these values, among the WT strains, sH1N1-WT had a higher proportion of virions with a high generation number compared to pH1N1-WT, H5N1-WT and H7N9-WT (Fig. 4A). pH1N1-PR8 also had a higher proportion of virions with a high generation number compared to H5N1-PR8 (Fig. 4B). To summarise this distribution, we calculated the mean generation number

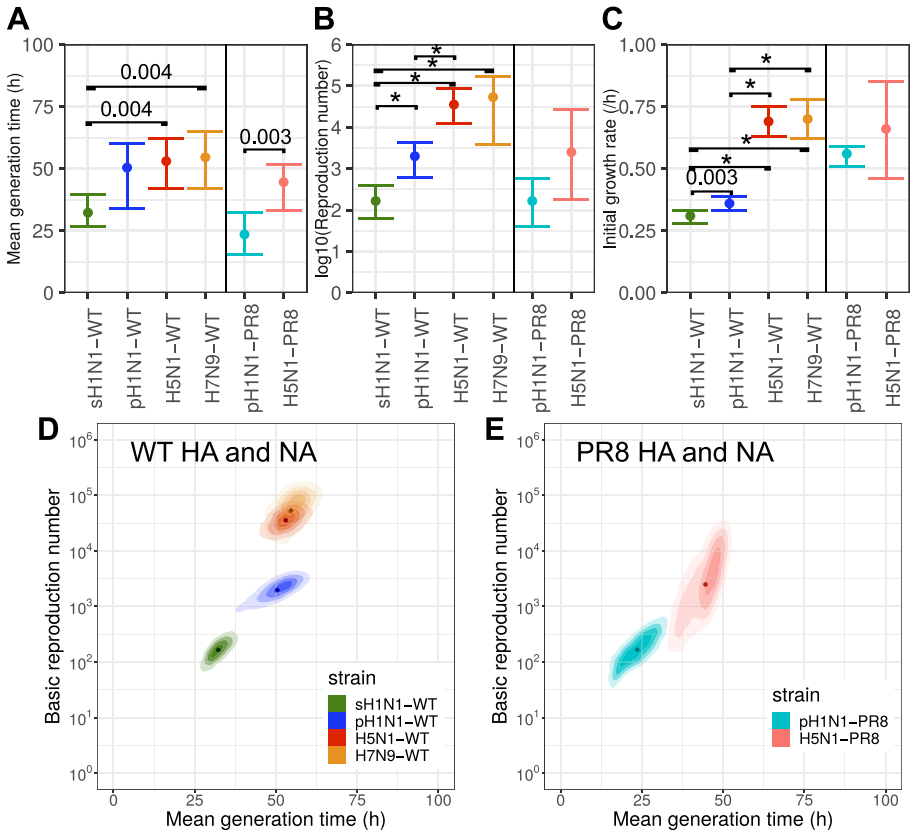

Fig. 3. Estimates for the mean generation time, basic reproduction number, and initial growth rate. (Top) The median and 95% credible intervals for (A) the mean generation time, (B) basic reproduction number, and (C) initial growth rate, for the wild-type (WT) strains (left of each panel), and the strains with PR8 HA and NA (right). Calculation of p-values is described in the Methods. Statistically significant pairs are labelled ($\alpha = 0.05$ with Bonferroni correction for seven pairwise tests per trait). Asterisks denote $p < 0.001$. (Bottom) Contour plots of the posterior density of the mean generation time and the basic reproduction number for each strain, for (D) the WT strains, and (E) the strains with PR8 HA and NA. Fainter shading indicates lower support; dots indicate median values.

at the time of peak infectious viral load. Calculating this statistic across the joint posterior distribution confirmed that strains with a lower basic reproduction number had a higher mean generation number, and thus virions were on average a product of more replication cycles (Fig. 4C).

We investigated the hypothesis that longer generation times alone might be driving the difference in number of replication cycles at peak viral shedding. However, we found that this was not the case. A sensitivity analysis showed that out of the three traits, changing the initial growth rate had the largest effect on the generation number distribution at the time of peak infectious viral load (Fig. 5). When we held the mean generation time constant (Fig. 5A), we were able to achieve very different generation number distributions by varying the other parameters. However, when we held the initial growth rate constant (Fig. 5C), varying the other parameters did not substantially change the generation number distribution. Hence, the initial growth rate was the main driver of the generation number distribution. Holding the basic reproduction number constant while varying the other parameters (Fig. 5B) led to more variation in the generation number distribution than when varying the generation time, but less than when varying the initial growth rate.

In Fig. 5, the traits were changed by varying p_{inf} and τ_I only. To consider the effect of all model parameters, we conducted Latin hypercube sampling of all model parameters across the 95% credible intervals obtained by fitting the model to the data. We then calculated the basic reproduction number, mean generation time initial growth rate and mean generation number for these samples, and used partial correlation coefficient analysis to determine the sensitivity of the mean generation number to each of these traits. The results, shown in Fig. S5, show that the mean generation number is most sensitive to the initial growth rate and least sensitive to the mean generation time, which is consistent with Fig. 5. Details of the methods are in Section 4 of the Supplementary Material.

We conducted a number of sensitivity analyses. We tested different model structures to see the impacts of model assumptions on the estimated values of traits. First, we ignored loss of free virions due to entry into target cells (Supplementary Material). These changes only changed estimated trait values slightly, and did not affect the relationship between the three traits, human adaptation, and the generation number distribution (Fig. S6). Second, we decreased the level of heterogeneity in the generation time. We first decreased heterogeneity by narrowing the distribution of the latent period and duration of virion production, by setting $n_L = n_I = 60$ in the model equations. This change also did not affect the above relationships (Fig. S7).

We then decreased heterogeneity by changing the timing of production of virions. In the model in the main text (Fig. 1, Eq. (1)), once each cell starts producing virus, it does so at a constant rate until death. (Note that due to heterogeneity in infected cells' lifetimes, the bulk production rate of virions by many cells varies over time.) On the other hand, models including intracellular processes predict an age-dependent production rate (Heldt et al., 2013). Fig. S8 shows the viral load estimated using a model where the production rate of virions increases over an infectious cell's age of infection (Supplementary Material). In this model, most virions are produced towards the end of an infected cell's lifespan, so there is less heterogeneity in the generation time. This model predicts slightly different dynamics from the model in the main text (Fig. 2). For the multi-cycle data, the new model predicts a sharp increase in viral load followed by a sharp decline for all strains. The model in the main text predicted similar dynamics for sH1N1-WT, pH1N1-WT and pH1N1-PR8, but a gradual plateau in viral load

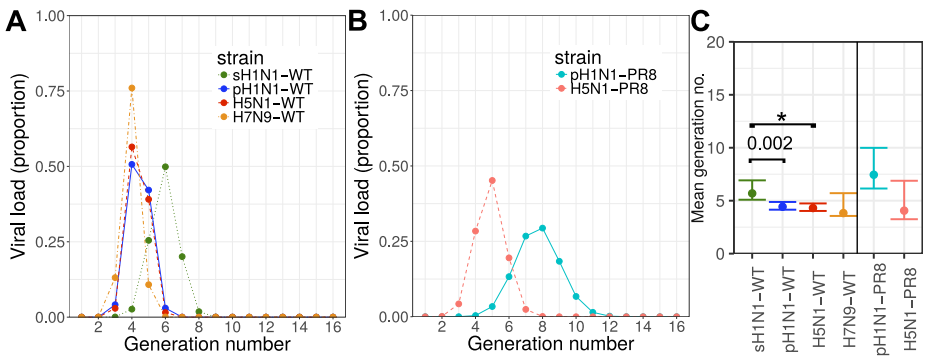

Fig. 4. Simulated distribution of the number of virions in each generation, for the six experimental strains. (A–B) The proportion of virions in each generation was calculated at the time of peak infectious viral load according to the maximum likelihood parameters for each strain, for (A) the WT strains, and (B) the strains with PR8 HA and NA. As visual aids, lines join the number of virions at each discrete generation. (C) The mean generation number was calculated for each sample from the joint posterior distribution for each strain. The median and 95% credible interval for the mean generation number are shown for the WT strains (left of each panel), and the strains with PR8 HA and NA (right). Statistically significant pairs are labelled ($\alpha = 0.05$ with Bonferroni correction for seven pairwise tests). Asterisks denote $p < 0.001$.

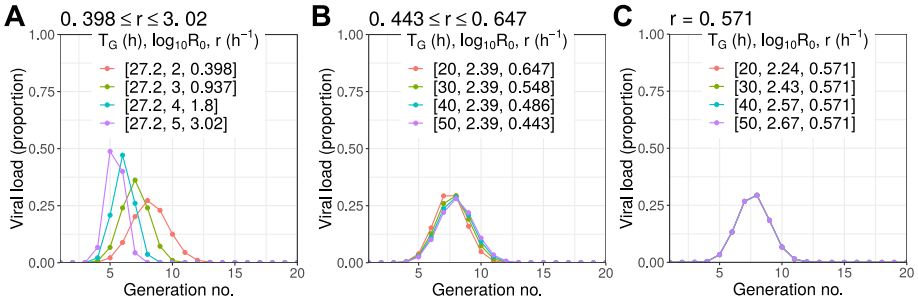

Fig. 5. Simulated distribution of the number of virions in each generation, as values of traits are changed systematically. The proportion of virions in each generation (the generation number distribution) was calculated at the time of peak infection. The traits in the legend were changed to the values shown. In each panel, one parameter is held constant: the mean generation time T_G (A), basic reproduction number R_0 (B), or initial growth rate r (C).

followed by a decrease for H5N1-WT, H7N9-WT and H5N1-PR8. This difference can be seen by inspection of the data, and is missed by the new model. For the single-cycle data, the new model produces "bumpy" curves with multiple stages of rapid viral growth, whereas the model in the main text produces the sigmoidal curves characteristic of single-cycle growth kinetics. Model predictions of the mock-yield viral load have a different slope from the data, particularly for H5N1-PR8. We hypothesise that in the new model, the slope of the multi-cycle viral load during its decay phase is less driven by the infected cell lifespan and more driven by the loss of virus infectivity; hence, the new model is unable to explain strain differences in the multi-cycle viral load decay rate without introducing artificial differences in the rate of loss of virus infectivity. Due to these qualitative differences between the data and the estimated viral load, we conclude that the model in the main text, where the production rate is constant, is more appropriate.

Last, we removed heterogeneity in the generation time altogether, which we hypothesised would change the relationship between the three traits and the number of replication cycles by the time of peak infectious viral load. We conducted this sensitivity analysis because evolutionary models often assume a fixed generation time, such that at a given time all virions belong to the same generation (Russell et al., 2012; Geoghegan et al., 2016; Illingworth, 2015). Fig. S8 shows the simulated generation number of virions at the time of peak infectious viral load for a model with a fixed generation time; details are given in the Supplementary Material. When we held the basic reproduction number constant (panel B in Fig. S9), varying the other parameters did not change the generation number, whereas when we held the generation time or the initial growth rate constant, we were able to change the generation number by varying the other parameters. Hence, for the fixed generation time model, only the basic reproduction number influences the generation number at the time of peak viral load. This drastically different result implies that quantitative predictions of the number of mutations accumulated during the time course of infection should account for heterogeneity in the generation time. This heterogeneity arises because virions are produced throughout the infectious period of a cell, and the infected cell lifespan is itself highly heterogeneous (Holder and Beauchemin, 2011; Beauchemin et al., 2017). These sources of heterogeneity are reflected in our model structure, and lead to successive generations of virions overlapping in time rather than all virions belonging to the same generation.

4. Discussion

By simultaneously estimating the basic reproduction number, the mean generation time, and the initial growth rate for *in vitro* influenza viral dynamics, our study has uncovered a novel positive correlation between these traits across six influenza A strains. Strain differences in the three traits were driven by changes in rates of different underlying infection processes, such that each trait provides a different perspective. Some studies have directly compared model parameter values for strains differing by a single mutation (Pinilla et al., 2012; Holder et al., 2011; Petrie et al., 2015; Simon et al., 2016). Because mutations may affect one or more infection processes captured by these parameters, combining these processes into a smaller number of traits – the basic reproduction number, mean generation time, and initial growth rate – may enable easier between-strain comparisons.

As reviewed by Wargo and Kurath (2012), virological data analysis protocols have mostly used the initial growth rate to measure *in vitro* fitness, interpreting a larger growth rate as a fitness advantage. The previous analysis of four of the strains presented here by Simon et al. (2016) showed strain differences in the rate of infection, which is closely related to the initial growth rate. A limited number of studies

have computed the basic reproduction number, and fewer still have compared it between virus strains (Mitchell et al., 2011; Iwanami et al., 2017; Farrukee et al., 2018). Some modelling studies have computed another related quantity, the infecting time, which is the time between a cell starting to produce virus and infection of the *first* secondary cell (Pinky and Dobrovolny, 2016; Paradis et al., 2015; Holder et al., 2011; Holder and Beauchemin, 2011; Pinilla et al., 2012; Petrie et al., 2013, 2015; Gonzàlez-Parra et al., 2018). The mean generation time differs from the infecting time because the mean generation time is averaged over *all* secondary cells, and also includes the period before an infected cell starts producing virus. If cell and virion loss are assumed to be negligible during early infection, then the initial growth rate is inversely proportional to the sum of the infecting time and the latent period before an infected cell produces virus.

The *in vitro* generation time has not previously been estimated for influenza using mechanistic models. The time to half-maximum viral load in a single-cycle experiment has been used as a heuristic estimate for the generation time by Nobusawa and Sato (2006), who estimated the generation time to be 7.6 h for A/1/87 and 9.7 h for B/29/99 — shorter than our estimates. However, the latter method depends on reliably capturing the peak viral load, and is thus sensitive to timepoints chosen; neglects loss of infectivity of infectious virus; and neglects the time taken for the viral progeny to infect a second cell. We propose that fitting mechanistic models to data is a more reliable method of estimating the generation time.

The estimated basic reproduction numbers range from 10^2 to 10^4 in orders of magnitude. Previous *in vitro* studies have estimated the basic reproduction number to range from 10^2 to 10^3 in orders of magnitude (Mitchell et al., 2011; Pinilla et al., 2012; Paradis et al., 2015), consistent with our work. *In vivo* studies have estimated lower basic reproduction numbers of order 10^1 (Baccam et al., 2006). This difference between *in vitro* and *in vivo* estimates could be due to true biological differences in the basic reproduction number, due to differences between the structure of the respiratory tract and cell culture (such as the mucus layer inhibiting infection in the respiratory tract, or greater spatial spread of the virus in the respiratory tract). They could also be due to innate and adaptive immunity curbing infection *in vivo* at the later stages of infection, which is not accounted for by target-cell limited models such as those by Baccam et al. (2006) — estimates using these models may underestimate the basic reproduction number.

We observe that the strains in our study with a low basic reproduction number, short mean generation time and slow growth rate are human-adapted (sH1N1-WT, pH1N1-WT and pH1N1-PR8), and those with a high basic reproduction number, long mean generation time and high growth rate (H5N1-WT, H7N9-WT and H5N1-PR8) are avian-adapted. These results suggest that the basic reproduction number, mean generation time and growth rate differ systematically between human-adapted and avian-adapted influenza strains. This finding held when virus surface proteins were standardised, suggesting that the differences are driven by internal proteins. The main limitation of our results with respect to this finding is that we have only assessed these traits in six strains. We note that experiments for two of the strains (pH1N1-PR8 and H5N1-PR8) were designed specifically to measure these traits and test the hypotheses generated using data from the other strains. Nonetheless, it would be desirable to repeat these experiments for a wider panel of strains with the same surface proteins, to see whether differences in traits still hold across more human-adapted and avian-adapted strains. If so, further investigation into the mechanisms driving these differences could lead to new methods to quantify human adaptation, to assess pandemic risk. Note that although the higher initial growth rate could be interpreted as a fitness advantage for avian-adapted strains in human cells, which is counterintuitive, in an *in vivo* situation, the immune response must be considered in addition to the initial growth rate. Moreover, the A549 cells used in these experiments have a higher proportion of receptors expressing α2-3-linked sialic acids compared to primary differentiated human airway epithelial cells, which may confer an advantage to avian-adapted strains in this cell type.

A previous study used primary normal human bronchial epithelial cells as a model of the respiratory tract, and found that higher, not lower, basic reproduction numbers were associated with human adaptation (Mitchell et al., 2011). Although this result appears to contradict our findings, higher basic reproduction numbers for human-adapted strains in primary normal human bronchial epithelial cells were likely due to strain differences in receptor binding specificity, since these cells primarily express α2,6-linked sialic acid receptors which are already well understood to be favoured by human-adapted strains. In our experiments where strains were engineered to have the same surface proteins, we could eliminate the already-known effects of receptor binding and isolate the effect of differences in internal proteins. If considering the combined effect of internal and surface proteins in wild-type strains, experimental conditions would need to more closely mimic conditions in the respiratory tract, for example by using primary differentiated human epithelial cells rather than the A549 cell line.

The same initial growth rate can be achieved with a small basic reproduction number and short generation time, or a large basic reproduction number and long generation time (Nishiura et al., 2010; Wallinga and Lipsitch, 2007). Correlation between the within-host basic reproduction number and mean generation time was also seen across patients in a previous study of HIV viral dynamics (Althaus et al., 2009), although the correlation was not commented upon in that study. The fact that some viruses have a small basic reproduction number and short generation time, and others have a large basic reproduction number and long generation time, suggests that these viruses may have different replication strategies. The difference between human-adapted and avian-adapted strains in this respect may reflect different replication strategies in the human respiratory tract and the avian gastrointestinal tract. To investigate this hypothesis, growth kinetics experiments could be conducted for the same strains in human and avian cell lines, and model parameter values could be compared between cell lines. For example, if we found that free virions lost infectivity more quickly in avian cell culture, a higher number of virions produced per infected cell could compensate.

The second finding of our study was that strains with lower basic reproduction numbers, shorter mean generation times and lower initial growth rates tend to have a higher proportion of virions which are a product of a large number of replication cycles at the time of peak infection, when transmission is most likely to occur for the *in vivo* case. Our analysis showed that the initial growth rate was the main driver of changes in the mean generation number, and that correlations between the basic reproduction number, mean generation time and mean generation number mainly arise through correlations between the initial growth rate, basic reproduction number, and mean generation time. For a given mutation rate per replication cycle (as estimated by Parvin et al. (1986) and Nobusawa and Sato (2006), this implies quicker accumulation of mutations. The degree of heterogeneity in the generation time also changed the generation number distribution. If we unrealistically assumed no heterogeneity in the generation time, then the generation number at the time of peak viral load depended entirely on the basic reproduction number rather than the initial growth rate, highlighting the importance of heterogeneity in the generation time in evolutionary models.

A caveat of this second finding is that the relationship between the generation number distribution and the initial growth rate would be different *in vivo* due to a time-dependent immune response. However, the overall finding that different parameter values lead to different generation number distributions at a given time should still hold. Also, in linking the accumulation of generations to accumulation of mutations, we have assumed that the number of errors introduced between primary and secondary virions is independent of when the secondary virion was produced during the infected cell's lifespan. However, the number of errors introduced may increase with the age of the infected

cell, since a virion exiting an 'older' cell may have been a product of more intracellular replication and transcription cycles than a virion exiting a 'younger' cell. In our model, we have not considered multiple intracellular replication and transcription cycles before virus release. However, the relationship between a cell's age and the number of mutations in produced virions is yet to be well understood.

CRediT authorship contribution statement

Ada W.C. Yan: Conceptualisation, Formal analysis, Methodology, Software, Visualisation, Writing - original draft, Writing - review & editing. **Jie Zhou:** Investigation, Methodology, Writing - original draft, Writing - review & editing. **Catherine A.A. Beauchemin:** Methodology, Resources, Visualisation, Writing - review & editing. **Colin A. Russell:** Conceptualisation, Funding acquisition, Writing - review & editing. **Wendy S. Barclay:** Conceptualisation, Funding acquisition, Methodology, Resources, Supervision, Writing - review & editing. **Steven Riley:** Conceptualisation, Formal analysis, Funding acquisition, Methodology, Project administration, Supervision, Visualisation, Writing - original draft, Writing - review & editing.

Declaration of competing interest

The authors declare that they have no known competing financial interests or personal relationships that could have appeared to influence the work reported in this paper.

Acknowledgements

This work was supported by a Wellcome Trust Collaborative Award (UK, https://wellcome.ac.uk/, grant 200187/Z/15/Z, AWCY, JZ, CAR, WSB and SR); a Wellcome Trust Investigator Award (UK, https://wellcome.ac.uk/, grant 200861/Z/16/Z, SR); a Discovery Grant 355-837-2013 from the Natural Sciences and Engineering Research Council of Canada (www.nserc-crsng.gc.ca, CAAB); Early Researcher Award ER13-09-040 from the Ministry of Research and Innovation and Science of the Government of Ontario (www.ontario.ca/page/early-researcher-awards, CAAB); and Interdisciplinary Theoretical and Mathematical Sciences (iTHEMS, ithems.riken.jp) at RIKEN (CAAB). We acknowledge joint Centre funding from the UK Medical Research Council and Department for International Development (https://mrc.ukri.org/, grant MR/R015600/1, AWCY and SR).

Appendix A. Supplementary data

Supplementary material related to this article can be found online at https://doi.org/10.1016/j.epidem.2020.100406.

References

Althaus, C.L., De Vos, A.S., De Boer, R.J., 2009. Reassessing the human immunodeficiency virus type 1 life cycle through age-structured modeling: Life span of infected cells, viral generation time, and basic reproductive number, R0. J. Virol. 83 (15), 7659–7667. http://dx.doi.org/10.1128/JVI.01799-08.

Baccam, P., Beauchemin, C., Macken, C.A., Hayden, F.G., Perelson, A.S., 2006. Kinetics of influenza A virus infection in humans. J. Virol. 80 (15), 7590–7599. http://dx.doi.org/10.1128/JVI.01623-05.

Beauchemin, C.A.A., Miura, T., Iwami, S., 2017. Duration of SHIV production by infected cells is not exponentially distributed: Implications for estimates of infection parameters and antiviral efficacy. Sci. Rep. 7, 42765. http://dx.doi.org/10.1038/srep42765.

Beggs, N.F., Dobrovolny, H.M., 2015. Determining drug efficacy parameters for mathematical models of influenza. J. Biol. Dyn. 9 (Suppl. 1), 332–346, PMID: 26056712 http://dx.doi.org/10.1080/17513758.2015.1052764.

Carrat, F., Vergu, E., Ferguson, N.M., Lemaitre, M., Cauchemez, S., Leach, S., Valleron, A.-J., 2008. Time lines of infection and disease in human influenza: a review of volunteer challenge studies. Am. J. Epidemiol. 167 (7), 775–785.

Dixit, N.M., Markowitz, M., Ho, D.D., Perelson, A.S., 2004. Estimates of intracellular delay and average drug efficacy from viral load data of HIV-infected individuals under antiretroviral therapy. Antivir. Ther. 9 (2), 237–246.

Farrukee, R., Zarebski, A.E., McCaw, J.M., Bloom, J.D., Reading, P.C., Hurt, A.C., 2018. Characterization of influenza B virus variants with reduced neuraminidase inhibitor susceptibility. Antimicrob. Agents Chemother. 62 (11), http://dx.doi.org/10.1128/AAC.01081-18.

Fonville, J.M., 2015. Expected effect of deleterious mutations on within-host adaptation of pathogens. In: Kirkegaard, K. (Ed.), J. Virol. 89 (18), 9242–9251. http://dx.doi.org/10.1128/JVI.00832-15.

Geoghegan, J.L., Senior, A.M., Holmes, E.C., 2016. Pathogen population bottlenecks and adaptive landscapes: overcoming the barriers to disease emergence. Proc. R. Soc. Lond. Biol. B 283 (1837), 20160727. http://dx.doi.org/10.1098/rspb.2016.0727.

Gonzàlez-Parra, G., De Ridder, F., Huntjens, D., Roymans, D., Ispas, G., Dobrovolny, H.M., 2018. A comparison of RSV and influenza in vitro kinetic parameters reveals differences in infecting time. In: Sun, J. (Ed.), PLoS One 13 (2), e0192645. http://dx.doi.org/10.1371/journal.pone.0192645.

González-Parra, G., Dobrovolny, H.M., Aranda, D.F., Chen-Charpentier, B., Guerrero Rojas, R.A., 2018. Quantifying rotavirus kinetics in the REH tumor cell line using in vitro data. Virus Res 244, 53–63. http://dx.doi.org/10.1016/j.virusres.2017.09.023.

Handel, A., Longini Jr., I.M., Antia, R., 2007. Neuraminidase inhibitor resistance in influenza: assessing the danger of its generation and spread. PLoS Comput. Biol. 3 (12), e240.

Heldt, F.S., Frensing, T., Pflugmacher, A., Gröpler, R., Peschel, B., Reichl, U., 2013. Multiscale modeling of influenza A virus infection supports the development of direct-acting antivirals. PLoS Comput. Biol. 9 (11), e1003372.

Holder, B.P., Beauchemin, C.A.A., 2011. Exploring the effect of biological delays in kinetic models of influenza within a host or cell culture. BMC Public Health 11 (Suppl. 1), S10.

Holder, B.P., Simon, P., Liao, L.E., Abed, Y., Bouhy, X., Beauchemin, C.A.A., Boivin, G., 2011. Assessing the in vitro fitness of an oseltamivir-resistant seasonal A/H1N1 influenza strain using a mathematical model. PLoS One 6 (3), e14767.

Illingworth, C.J., 2015. Fitness inference from short-read data: Within-host evolution of a reassortant H5N1 influenza virus. Mol. Biol. Evol. 32 (11), 3012–3026. http://dx.doi.org/10.1093/molbev/msv171.

Iwami, S., Holder, B.P., Beauchemin, C.A., Morita, S., Tada, T., Sato, K., Igarashi, T., Miura, T., 2012. Quantification system for the viral dynamics of a highly pathogenic simian/human immunodeficiency virus based on an in vitro experiment and a mathematical model. Retrovirology 9 (1), 18. http://dx.doi.org/10.1186/PREACCEPT-8502330256154242.

Iwami, S., Takeuchi, J.S., Nakaoka, S., Mammano, F., Clavel, F.c., Inaba, H., Kobayashi, T., Misawa, N., Aihara, K., Koyanagi, Y., Sato, K., 2015. Cell-to-cell infection by HIV contributes over half of virus infection. In: Chakraborty, A.K. (Ed.), eLife 4, e08150. http://dx.doi.org/10.7554/eLife.08150.

Iwanami, S., Kakizoe, Y., Morita, S., Miura, T., Nakaoka, S., Iwami, S., 2017. A highly pathogenic simian/human immunodeficiency virus effectively produces infectious virions compared with a less pathogenic virus in cell culture. Theor. Biol. Med. Model. 14 (1), 9. http://dx.doi.org/10.1186/s12976-017-0055-8.

Koelle, K., Farrell, A.P., Brooke, C.B., Ke, R., 2019. Within-host infectious disease models accommodating cellular coinfection, with an application to influenza. Virus Evol. 5 (2), http://dx.doi.org/10.1093/ve/vez018.

Lee, H.Y., Topham, D.J., Park, S.Y., Hollenbaugh, J., Treanor, J., Mosmann, T.R., Jin, X., Ward, B.M., Miao, H., Holden-Wiltse, J., Perelson, A.S., Zand, M., Wu, H., 2009. Simulation and prediction of the adaptive immune response to influenza a virus infection. J. Virol. 83 (14), 7151–7165. http://dx.doi.org/10.1128/JVI.00098-09.

Liao, L.E., Iwami, S., Beauchemin, C.A.A., 2016. (In)validating experimentally derived knowledge about influenza A defective interfering particles. J. R. Soc. Interface 13 (124), http://dx.doi.org/10.1098/rsif.2016.0412.

Lyons, D., Lauring, A., 2018. Mutation and epistasis in influenza virus evolution. Viruses 10 (8), 407. http://dx.doi.org/10.3390/v10080407.

Mitchell, H., Levin, D., Forrest, S., Beauchemin, C.A.A., Tipper, J., Knight, J., Donart, N., Layton, R.C., Pyles, J., Gao, P., Harrod, K.S., Perelson, A.S., Koster, F., 2011. Higher level of replication efficiency of 2009 (H1N1) pandemic influenza virus than those of seasonal and avian strains: kinetics from epithelial cell culture and computational modeling. J. Virol. 85 (2), 1125–1135. http://dx.doi.org/10.1128/JVI.01722-10.

Möhler, L., Flockerzi, D., Sann, H., Reichl, U., 2005. Mathematical model of influenza a virus production in large-scale microcarrier culture.. Biotechnol. Bioeng. 90 (1), 46–58. http://dx.doi.org/10.1002/bit.20363.

Nené, N.R., Dunham, A.S., Illingworth, C.J.R., 2018. Inferring fitness effects from time-resolved sequence data with a delay-deterministic model. Genetics 209 (1), 255–264. http://dx.doi.org/10.1534/genetics.118.300790.

Nishiura, H., Chowell, G., Safan, M., Castillo-Chávez, C., 2010. Pros and cons of estimating the reproduction number from early epidemic growth rate of influenza A (H1N1) 2009. Theor. Biol. Med. Model. 7 (1), 1–13. http://dx.doi.org/10.1186/1742-4682-7-1.

Nobusawa, E., Sato, K., 2006. Comparison of the mutation rates of human influenza A and B viruses. J. Virol. 80 (7), 3675–3678. http://dx.doi.org/10.1128/JVI.80.7.3675.

Nowak, M.A., Bangham, C.R.M., 1996. Population dynamics of immune responses to persistent viruses. Science 272 (5258), 74–79. http://dx.doi.org/10.1126/science.272.5258.74.

Nowak, M.A., Lloyd, A.L., Vasquez, G.M., Wiltrout, T.A., Wahl, L.M., Bischofberger, N., Williams, J., Kinter, A., Fauci, A.S., Hirsch, V.M., Lifson, J.D., 1997. Viral dynamics of primary viremia and antiretroviral therapy in simian immunodeficiency virus infection. J. Virol. 71 (10), 7518–7525.

Paradis, E.G., Pinilla, L.T., Holder, B.P., Abed, Y., Boivin, G., Beauchemin, C.A.A., 2015. Impact of the H275Y and I223V mutations in the neuraminidase of the 2009 pandemic influenza virus in vitro and evaluating experimental reproducibility. PLoS One 10 (5), 1–24. http://dx.doi.org/10.1371/journal.pone.0126115.

Parvin, J.D., Moscona, A., Pan, W.T., Leider, J.M., Palese, P., 1986. Measurement of the mutation rates of animal viruses: influenza A virus and poliovirus type 1. J. Virol. 59 (2), 377–383.

Perelson, A.S., Neumann, A.U., Markowitz, M., Leonard, J.M., Ho, D.D., 1996. HIV-1 dynamics in vivo: Virion clearance rate, infected cell life-span, and viral generation time. Science 271 (5255), 1582–1586. http://dx.doi.org/10.1126/science.271.5255.1582.

Petrie, S.M., Butler, J., Barr, I.G., McVernon, J., Hurt, A.C., McCaw, J.M., 2015. Quantifying relative within-host replication fitness in influenza virus competition experiments. J. Theoret. Biol. 382, 259–271. http://dx.doi.org/10.1016/j.jtbi.2015.07.003.

Petrie, S.M., Guarnaccia, T., Laurie, K.L., Hurt, A.C., McVernon, J., McCaw, J.M., 2013. Reducing uncertainty in within-host parameter estimates of influenza infection by measuring both infectious and total viral load. PLoS One 8 (5), e64098. http://dx.doi.org/10.1371/journal.pone.0064098.

Pinilla, L.T., Holder, B.P., Abed, Y., Boivin, G., Beauchemin, C.A.A., 2012. The H275Y neuraminidase mutation of the pandemic A/H1N1 influenza virus lengthens the eclipse phase and reduces viral output of infected cells, potentially compromising fitness in ferrets. J. Virol. 86 (19), 10651–10660.

Pinky, L., Dobrovolny, H.M., 2016. Coinfections of the respiratory tract: Viral competition for resources. In: Tripp, R. (Ed.), PLoS One 11 (5), e0155589. http://dx.doi.org/10.1371/journal.pone.0155589.

Reperant, L.A., Grenfell, B.T., Osterhaus, A.D.M.E., 2015. Quantifying the risk of pandemic influenza virus evolution by mutation and re-assortment. Vaccine 33 (49), 6955–6966. http://dx.doi.org/10.1016/j.vaccine.2015.10.056.

Russell, C.A., Fonville, J.M., Brown, A.E.X., Burke, D.F., Smith, D.L., James, S.L., Herfst, S., van Boheemen, S., Linster, M., Schrauwen, E.J., Katzelnick, L., Mosterin, A., Kuiken, T., Maher, E., Neumann, G., Osterhaus, A.D.M.E., Kawaoka, Y., Fouchier, R.A.M., Smith, D.J., 2012. The potential for respiratory droplet-transmissible A/H5N1 influenza virus to evolve in a mammalian host. Science 336 (6088), 1541–1547. http://dx.doi.org/10.1126/science.1222526.

Sanjuán, R., 2010. Mutational fitness effects in RNA and single-stranded DNA viruses: common patterns revealed by site-directed mutagenesis studies. Phil. Trans. R. Soc. B 365 (1548), 1975–1982. http://dx.doi.org/10.1098/rstb.2010.0063.

Simon, P.F., de La Vega, M.-A., Paradis, É., Mendoza, E., Coombs, K.M., Kobasa, D., Beauchemin, C.A.A., 2016. Avian influenza viruses that cause highly virulent infections in humans exhibit distinct replicative properties in contrast to human H1N1 viruses. Sci. Rep. 6 (1), 24154. http://dx.doi.org/10.1038/srep24154.

Wallinga, J., Lipsitch, M., 2007. How generation intervals shape the relationship between growth rates and reproductive numbers. Proc. R. Soc. Lond. Biol. 274 (1609), 599–604. http://dx.doi.org/10.1098/rspb.2006.3754, http://rspb.royalsocietypublishing.org/cgi/doi/10.1098/rspb.2006.3754.

Wargo, A.R., Kurath, G., 2012. Viral fitness: definitions, measurement, and current insights. Curr. Opin. Virol. 2 (5), 538–545. http://dx.doi.org/10.1016/j.coviro.2012.07.007.